MEASUREMENTS OF THE LiCAS SYSTEM

P. Baker, R. Bingham, C. Glasman, J. Green, G. Grzelak,
A. Mitra, J. Nixon C. Perry, A. Reichold
University of Oxford, UK
J. Prenting, M. Schlösser
Applied Geodesy Group, DESY, Germany

1 INTRODUCTION

The Linear Collider requires precision survey and alignment during construction and operation. The TESLA collider is one proposed design with a vertical alignment tolerance of 200 μm over 600 m and a horizontal alignment tolerance of 500 μm over 600 m [1]. This demanding tolerance cannot be achieved with conventional surveying techniques which are limited by the refraction of light in air. The Linear Collider Alignment and Survey (LiCAS) group in collaboration with the DESY applied geodesy group have been developing a Rapid Tunnel Reference Surveyor (RTRS) to overcome the limitations of conventional surveying techniques [2]. The LiCAS group has been developing novel optical metrology techniques. The status of the laboratory test systems is discussed in this paper. There is an additional paper describing the simulation and performance of the LiCAS system inside the RTRS [3].

1.1 Overview of the RTRS and the LiCAS measurement system

A proposed procedure to survey and align the Linear Collider is to first survey a reference network attached to the tunnel wall. Then in a second step, one surveys reference markers attached to the accelerator with respect to the reference network [2]. The RTRS is being developed to perform the survey of the reference network in a series of overlapping steps [2]. The second step is performed with a laser tracker [1].

The RTRS consists of 6 cars which perform measurements between neighbouring cars and reference markers [2] attached to the accelerator tunnel wall. The measurements between the cars are performed by a set of 5 m Frequency Scanning Interferometers (FSI) and the Laser Straightness Monitors (LSM) (figure 1). The FSI lines measure the distance between cars and has some sensitivity to the relative orientations between cars. The LSM is able to measure the cars distance and orientation with respect to a laser beam which runs through

[1] Another proposal is to attach a steerable FSI line to replace the laser tracker. This unit could be attached to the RTRS.

[2] The reference markers are sphere mounted retroreflectors.

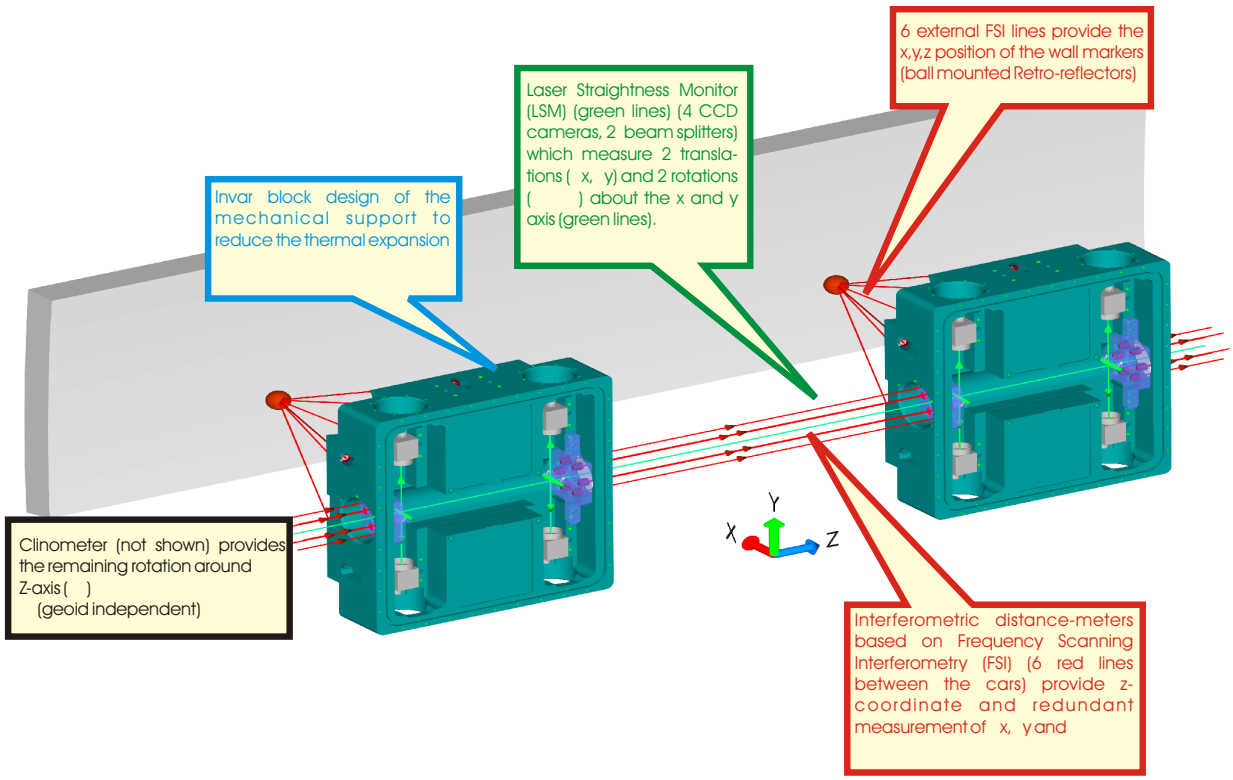

Figure 1: The LiCAS RTRS Survey Train: Two of the six LiCAS units of the RTRS are shown in the figure. The LiCAS units are fitted into a support frame (not shown). The LiCAS units has two "internal" systems: FSI and the LSM. The LSM is shown in green and the internal FSI lines are in red. All the internal systems are in vacuum and so there is a vacuum pipe (not shown) between cars. The vacuum pipe connects to the cars through universal joints and vacuum bellows. Measurements to the reference markers are made 6 "external" FSI lines arranged in a cone. These measurements are in open air but the distances are short ($\approx 40\,\mathrm{cm}$). So monitoring the air temperature and temperature will be sufficient to correct for the air refractive index. There is an inclinometer (not shown) which measures rotations about the z axis.

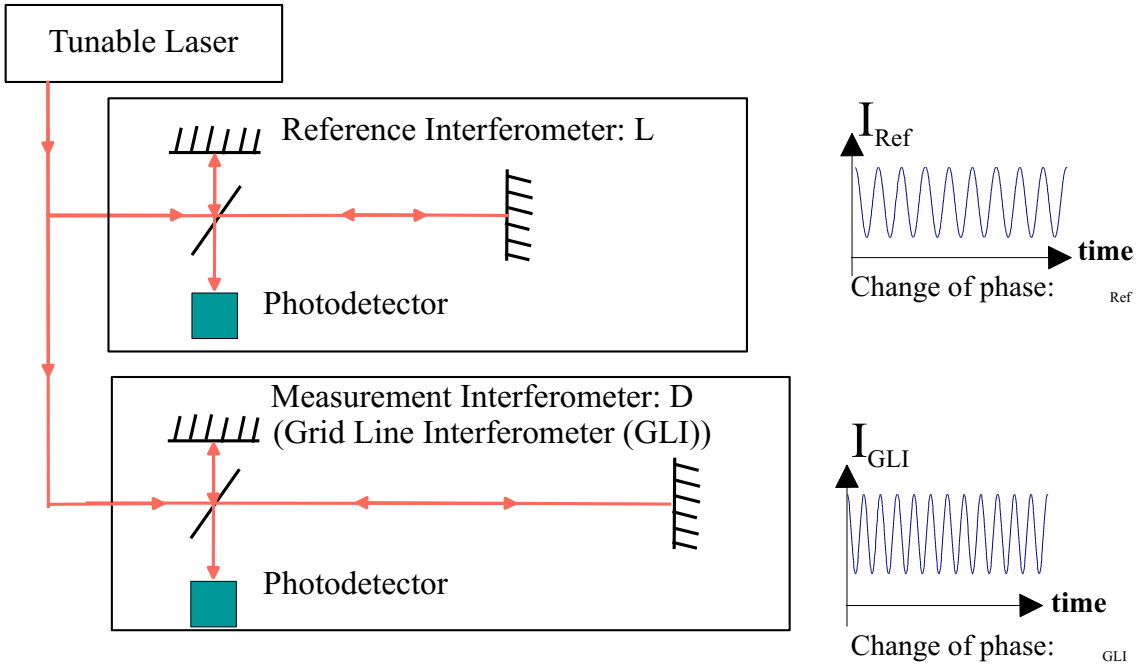

Figure 2: Light from a tunable laser illuminates a reference interferometer of known length L and a measurement interferometer of unknown length D. The laser sweeps through a frequency range which induces phase shifts in the interferometers. The interferometer signals are recorded and the change in phase is measured. The ratio of the induced phase changes of the interferometers is equal to the ratio of interferometer lengths.

all the RTRS' cars. These "internal measurements" are all performed inside a vacuum to avoid air refraction problems.

The measurements of the cars to the tunnel wall markers are performed by a set of 6 open air FSI lines in the form of a cone. The combination of the lines measures the 3D position of the reference marker. The external air temperature and pressure are monitored to correct the air refractive index. However as the lines are short ($\approx$ 40 cm), so the corrections are small.

2 FREQUENCY SCANNING INTERFEROMETRY (FSI)

Frequency Scanning Interferometry is an interferometric length measurement technique capable of making multiple, simultaneous measurements to an accuracy of 1 μm over 5 m [4] [5] [6] [7].

Figure 2 illustrates the FSI measurement technique. There is a reference interferometer of know length L and a Grid Line Interferometer (GLI) of unknown length D. Both are connected to a tunable laser [3] As the laser tunes, it induces phase shifts in the interferometers which are observed as sinusoidal variations of power at the photodetectors. These signals are recorded and the change in phase is measured. The ratio of interferometers lengths is equal to the ratio of phase change in the interferometers (equation 1).

$$\frac{D}{L} = \frac{\Delta\Phi_{GLI}}{\Delta\Phi_{Ref}} \tag{1}$$

2.1 FSI DAQ & Optics

Over the past decade the Telecoms market has developed high quality optical equipment which is cheap and readily available. The LiCAS group is exploiting this market to develop a scalable FSI system.

A key technology of the Telecoms market is the Erbium Doped Fibre Amplifier (EDFA) [10]. It is an optical amplifier which operates at the Telecoms wavelength [4]. It can amplify the 1 mW from the low power tunable laser to 100 mW which is sufficient to power a large array of GLIs. This allows a scalable, cost effective solution.

The FSI analysis algorithms work best when the fringes are sampled well. The fastest FSI fringe rate comes from the 5 m inter-car line which has a fringe rate of ≈166 KHz. For a base-line sample rate of 10 samples per fringe, the base-line DAQ rate is 1.7 MHz. This large sample rate has lead to the design of custom high speed ADC boards which under development. In addition a high speed bus is required to transfer the sampled ADC data to the PC's RAM. USB 2.0 has been chosen as bus to connect the custom DAQ board to the PC which has a transfer rate of 60 MB/s [11]; sufficient for the high speed FSI DAQ rates.

2.2 FSI interferometer design

2.2.1 Grid Line Interferometer (GLI) design

Figure 3 shows a LiCAS GLI. It a fibre coupled common path interferometer which consists of two parts: the Quill and retroreflector. The quill is the interferometer head which holds a collimator lens and a glass beam splitter. A single-mode, angled polished fibre screws into the end of the quill. The retroreflector forms the other half of the GLI. The measured distance is from the end of the quill to the retroreflector. Currently the quill is a commercial collimator with a glass window glued to the end. Studies are in progress to improve upon the commercial design.

[3] Tunable laser: a laser whose wavelength can be adjusted.
[4] Telecoms wavelength: 1520 nm to 1620 nm

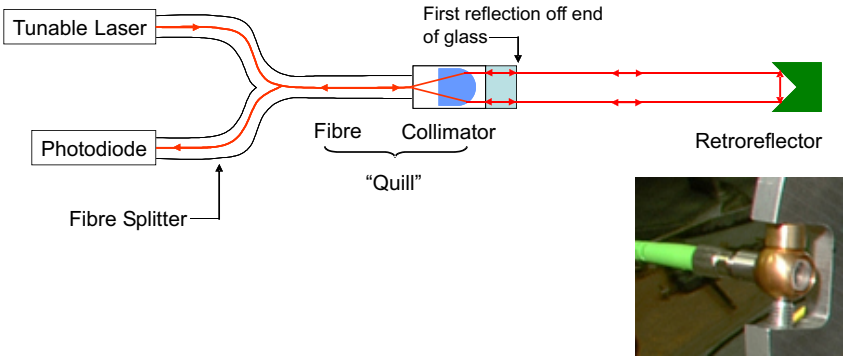

Figure 3: The LiCAS FSI GLI Interferometer: The interferometer consists of two parts: the Quill and retroreflector. The Quill body holds the collimator and a glass beam splitter. The retroreflector forms the other half of the GLI. The measured distance is from the end of the quill to the retroreflector. The photograph on the right is a complete quill. The end of the fibre screws into the quill. The glass beam splitter can be seen just protruding out of the holder.

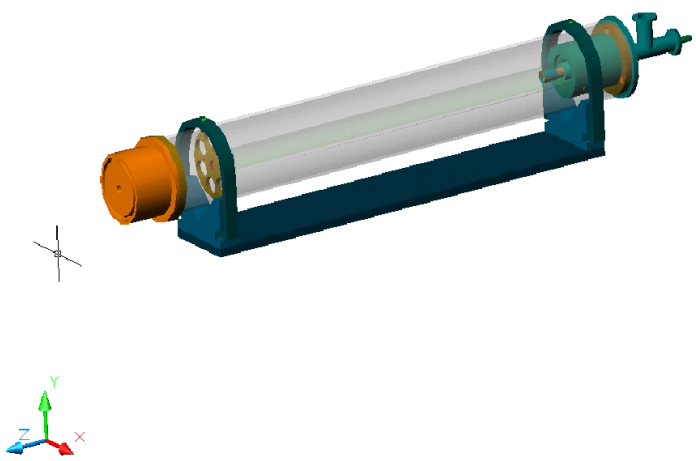

Figure 4: Rendered CAD Image of the "GLI-Style" reference interferometer inside it vacuum tube which is transparent for clarity in this figure.

2.2.2 Reference interferometer design

The reference interferometer is one of the critical components of the FSI system as it is the "yard-stick" for the entire system. Thus the interferometer length must remain constant irrespective of changes in temperature, pressure, vibration, etc.

A proposed design is to use a temperature compensated "GLI-style" interferometer inside a vacuum chamber (figure 4). This allows a compact reference interferometer which can be made rigid, robust and insensitive to the relative alignment of the internal components. This is particularly suited for use inside the RTRS.

The two ends of the interferometer are held inside a steel tube and the retroreflector is mounted on a nylon thread. Nylon has a coefficient of thermal expansion which is ≈10 times that of steel. As the external temperature varies, the steel tube will expand but the Nylon thread will also expand to compensate for the expansion. So the length of the interferometer remains constant. The whole interferometer is placed into a vacuum tube to avoid air refraction problems.

The components for the reference interferometer are currently in production. In the meantime a 2 m Michelson interferometer fixed to an optical table serves as the reference interferometer.

2.3 FSI data analysis

The conversion from interferometer signal to a length follows two steps:

1. The raw data from the interferometer is the photodetector intensity as a function of time. The interferometer phase is extracted from the raw data to give the interferometer phase as a function of time.

2. The reference and GLI phase are plotted together by matching phase points with the same time stamp. The graph is fitted to a straight line and the gradient gives the ratio of the phase advance of the interferometers which is equal to the ratio of the interferometer lengths.

2.3.1 Phase Extraction

An FSI length measurement relies on measuring the interferometer phase advance accurately. A standard technique for measuring the phase of an interferometer signal is the Carré algorithm [5]. This is a method of taking 4 measurements to solve a set of simultaneous equations to determine the phase. The only condition for the Carré algorithm is each point must be equally separated in phase. The optimum phase separation between points is $\approx 110°$.

Analysis routines have been developed to select points which are separated by $\approx 110°$. A sliding window is placed over the data set and the number of fringes in that window are counted. As the number of data points in the window are known, the separation of points for 110° interferometer phase change can be set.

2.4 Results from FSI

2.4.1 Laser tuning

The first test of the Telecoms laser was to measure its tuning linearity with time. The laser was tuned from 1535 nm to 1565 nm and and fed into a Michelson interferometer. The extracted interferometer phase is plotted in figure 5. The raw data (in black) is fitted to a straight line (in red) and appears to tune linearly. However the difference of the data and fit shows the tuning curve is slightly non linear (figure 6). A closer inspection of this graph reveals a sinusoidal-like fine structure.

The parabola should be expected as the laser tunes linearly in wavelength rather than frequency. However the fine structure is likely to be a property of the laser as another similar laser exhibits similar behaviour. It is believed the laser tuning feedback mechanism is responsible. Despite these non linear affects do not effects the FSI measurement are not affected.

2.4.2 Measurements of a 42 cm GLI

A 42 cm GLI was set-up with the retroreflector placed on a stage perpendicular to the beam. The stage was adjusted to move the retroreflector and and a set of FSI measurements were taken at each stop. The mean of the set was taken as the length and the RMS defined the error on the measurement. The results are plotted in figure 7.

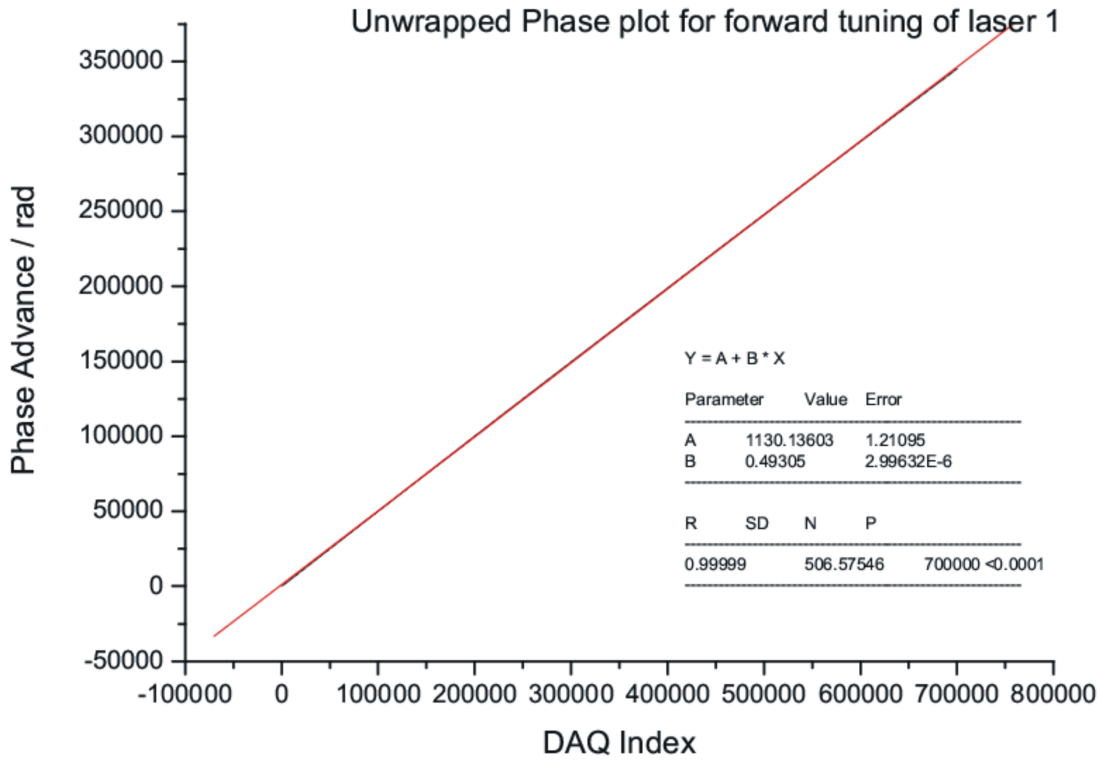

Figure 5: Laser tuning curve for the tunable laser. The data was plotted (black points) and fitted to a straight line (red line) The results of the fit are shown in the figure. It appears the laser tunes linearly but the figures below show otherwise.

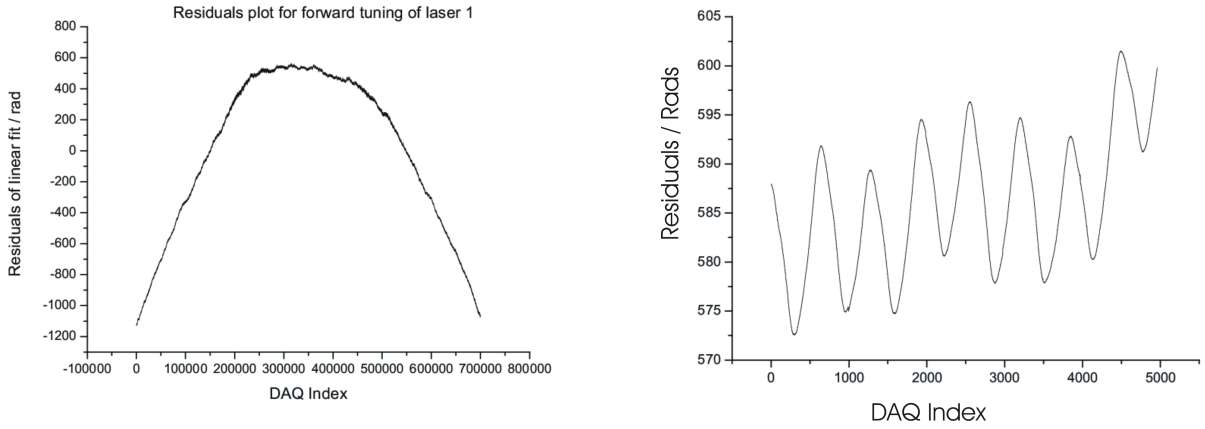

Figure 6: Residuals of the tuning curve and the linear fit. The left-hand graph shows the tuning curve has a small non-linear component. The right-hand graph is a zoomed in section of the left-hand graph. There is an additional small scale sinusoidal structure within the tuning curve. The origin of this structure could be due to the laser's tuning feedback mechanism.

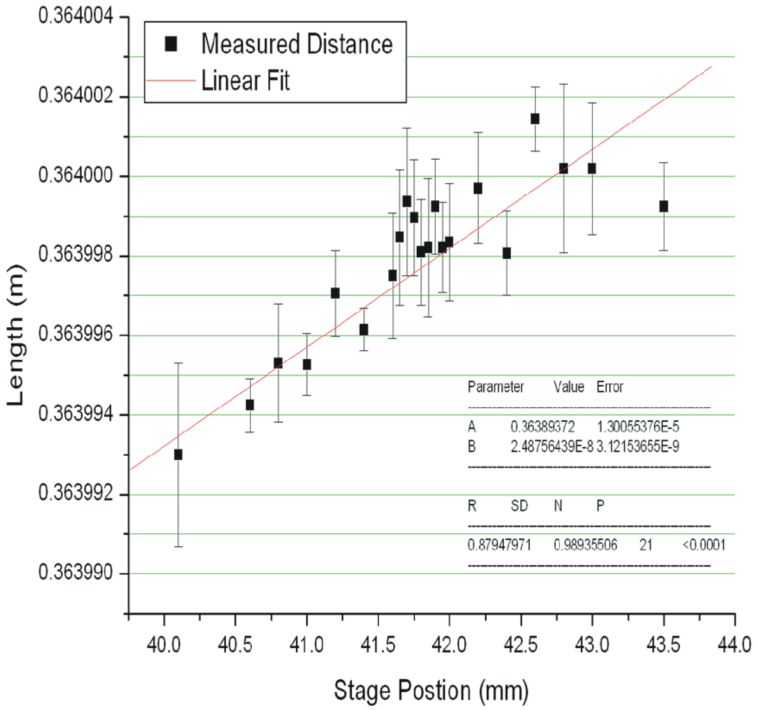

Figure 7: Results of a 42 cm GLI. At each stage positions a set of FSI measurements were made. The mean of the set is taken as the length and the RMS is error. The retro was placed on a stage perpendicular to the GLI. One would expect the results to follow a parabola. Instead a straight line is seen which suggests the stage was at an angle to the GLI.

If the stage was exactly perpendicular to the beam, one would expect the measured length to vary as a parabola as a function of stage position. Instead a straight line was observed. This suggests the stage was at angle to the beam.

This set of measurements was the first attempt to perform a LiCAS FSI measurement. Although the required 1 μm accuracy was not reached, the $\mathcal{O}(4\,\mu\text{m})$ error is encouraging. It is expected improvements in the reference interferometer, temperature monitoring, and analysis will reduce the errors.

3 LASER STRAIGHTNESS MONITOR (LSM)

The Laser Straightness Monitor (LSM) is an optical analogue of a stretched wire used in accelerator alignment. A laser beam passes through all the cars of the RTRS and each car measures its displacement and orientation with respect to this beam.

Each car of the RTRS has a pair of beam-splitters which intercept the LSM beam (figure 1 & figure 8). The reflected beams are seen by a pair of CCD cameras. At the end car of the RTRS, the LSM beam is reflected back by a retroreflector. This reflected beam re-intercepts the beam-splitters in the cars. The second reflections are registered by a second pair of CCD

cameras. Each CCD is capable of measuring the reflected beam-spot position to 1 μm. The combination of the 4 beam positions defines a unique car position and orientation.

3.1 LSM optics

The choice of laser is important for the LSM. A laser with transverse coherence but low longitudinal coherence is used. This allows efficient coupling into a single-mode optical fibre but removes interference from spurious reflections.

A typical beam-splitter is a few millimetres thick and one observes reflections off the front and back surface. This is not suitable for the LSM as the two reflections could not be easily distinguished. For the LSM, Pellicle beam-splitters are used. They are 4 μm thick stretched Nitrocellulose membranes, so only one reflection is observed [12].

3.2 LSM Test Hardware

3.2.1 Beam Stability

The beam stability was tested by monitoring its position with a camera. It was found the beam stability was $< 1\,\mu$m (figure 10). This satisfies the requirements for LSM.

3.2.2 Two degrees-of-freedom (DOF) test system

A half LSM [5] were placed on a linear translation stage and rotation stage (figure 9). The half-LSM was translated and rotated. Each stage position was recorded along with the beam images from the cameras. The half-LSM behaved as expected and the results are plotted in figure 11.

3.2.3 Four degrees-of-freedom test system

The LSM is capable of measuring two translations and two rotations. An LSM was placed on a set of stages which can provide all these motions (figure 12). In addition to the LSM stages, the retroreflector is placed on a pair of crossed stages to allow one to vary the retroreflector walk.

The LSM stages are mounted on high precision sub-micron and sub micro-radian stages. This exceeds the the resolution required for the RTRS. This will allow the LSM sensitivity to be measured. The sensitivity will be measured by moving the LSM through small increments and comparing the reconstructed LSM position with the stage readings.

3.3 Calibration and Reconstruction

Figure 11 has shown the CCD can register the motions of the LSM. However for the RTRS, the LSM must be able to provide the car's position and orientation from the recorded beam

[5] 1 beam-splitter & 2 CCD cameras

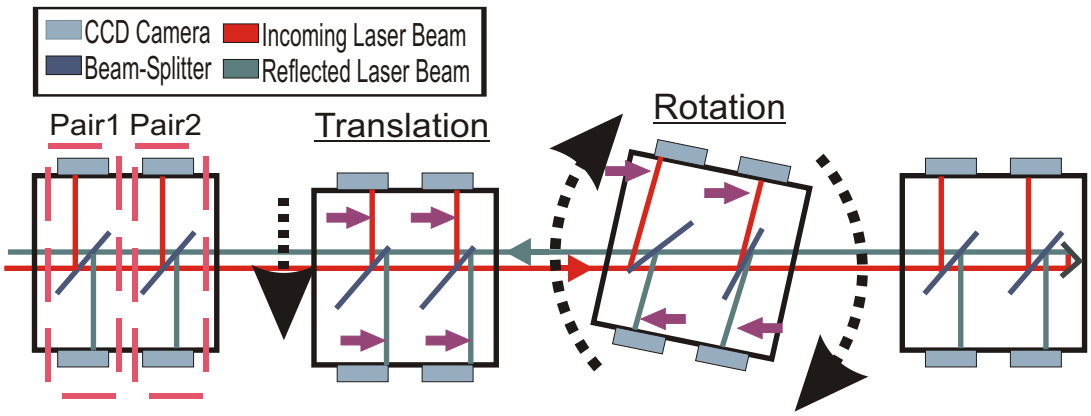

Figure 8: The Laser Straightness Monitor (LSM): Four of the six cars of the RTRS are shown. The LSM measures each car's position and orientation with respect to the LSM beam. The LSM beam passes twice through every car: once on the initial pass and a second after being reflected by the retroreflector in the end car. Each car has a pair of beam splitters. The reflections are registered by 4 cameras in each car. Each position of the reflected beams on the 4 CCDs define a unique car position and orientation. The figure shows for a pure translation all the reflected beam spots move in the same direction. For a pure rotation, the reflected beams for each pair of cameras move in opposite directions.

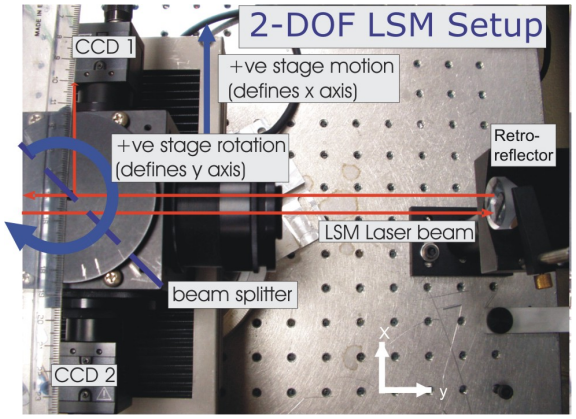

Figure 9: The 2 DOF LSM system. A half-LSM is placed on a translation and rotation stage. The stages move the half-LSM and the CCD images are recorded at each stage position.

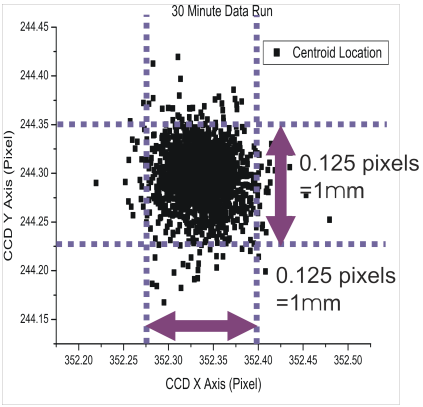

Figure 10: The figure shows the variation of the LSM beam position over a 30 minute period. The bound of the scatter are within 1 μm which satisfies the requirements as an LSM source.

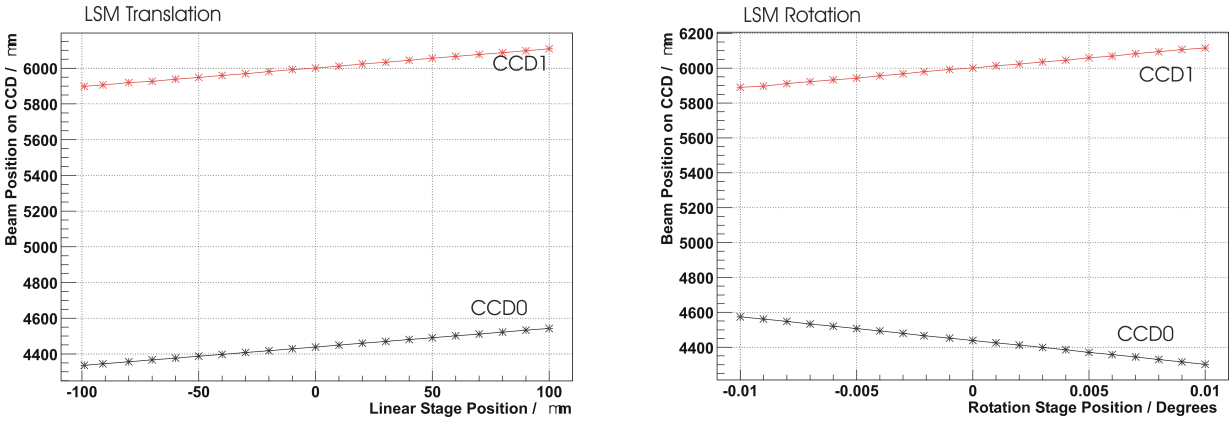

Figure 11: Results from the 2 DOF LSM system. The left-hand graph shows the LSM translation, with the beam spots moving in the same direction. The right-hand graph shows the LSM rotation as the beam spots move in opposite directions.

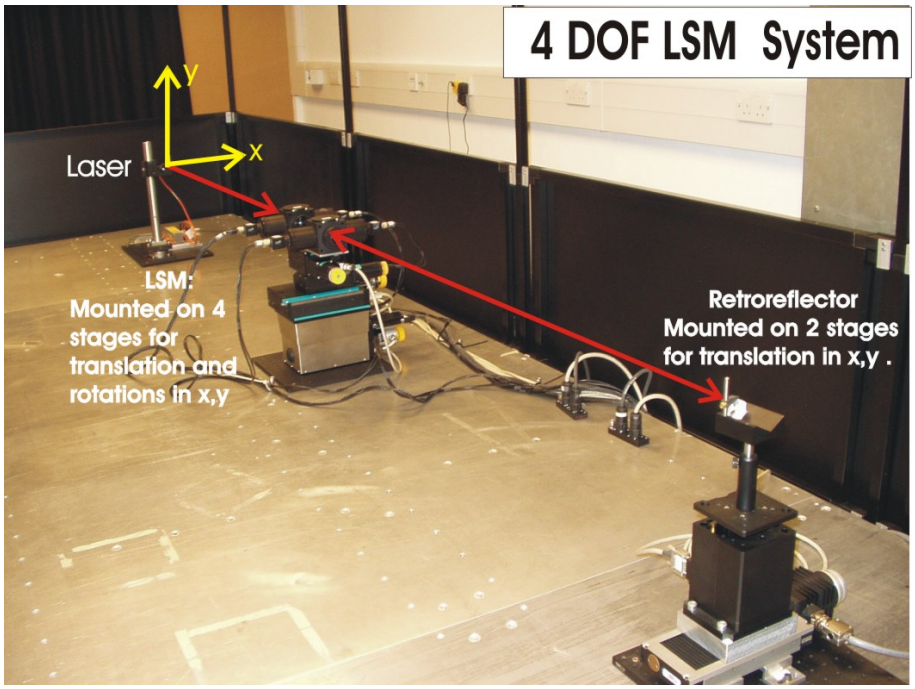

Figure 12: The 4 DOF LSM System: The LSM is place on 4 stages to translate the LSM in x, y and rotate it about x, y. In addition, the retroreflector is mounted on an x, y translation stage. This allows the retroreflector walk to be varied. This setup will allow the LSM sensitivity and calibration to be measured.

positions. This requires an accurate model of the internal geometry of the LSM; each beam-splitter and camera's position and orientation has to be measured. The LSM must be calibrated.

Attempting the calibration with an external system is not feasible as the CCDs are not externally accessible in their final position. Also the pellicle beam splitter is very delicate and cannot be touched.

The high precision stages of the 4 DOF LSM stand (figure 12) can be used to calibrate the LSM in situ. The LSM can be moved through a series of high precision differential translations and rotations and the beam positions on the cameras are recorded for each stage position. By analysing how the beam position moves for the 4 camera as the stages move; one can relate this to the internal geometry of the LSM. For example, a beam-splitter at 45° would displace a beam on a CCD the same amount as an unrotated LSM is translated. Any deviations from this would relate to a different beam splitter angle.

One method to extract the calibration constants is to use a fitting programme which has a model of the LSM. This has been implemented in SIMULGEO [8] and some success with this approach has been achieved. Further details of this procedure can be found in [3].

3.3.1 LSM Neural Net Calibration and Reconstruction

An approach to avoid calibration is to have a function which parameterises the mapping of the recorded beam positions to LSM position and orientation as a set of effective parameters. A Neural Net can be used to derive this parameterisation.

Data from the 4-DOF LSM setup is fed to the Neural Net as a set of training data. The Neural Net learns to associate beam positions with a given stage position. As more data is fed to the Neural Net, it develops a set of effective parameters to map the beam positions to LSM positions.

The effectiveness of the Neural Net has been tested using the Neural Net object defined in the ROOT [9] data analysis package. It was fed data from an LSM simulation and trained to associate beam positions with an LSM position and orientation. After the training session the Neural Net was fed with the beam positions from the simulation to reconstruct the LSM position. A graph showing the results is shown in figure 13. It shows the Neural Net has been successful in reconstructing the position of one of the LSM's CCD.

The current LSM model in the simulation has been simple with all the components in their ideal position. The next step would be to make the simulation more realistic by moving the LSM components off their ideal position and adding noise to the data.

4 CONCLUSIONS

Since the last IWAA meeting the hardware and analysis of the LiCAS systems has progressed well. Both systems work as a proof of principal. The next stage is to develop the systems to realising the required precision for LiCAS and the RTRS.

The use of Telecoms lasers and EDFAs has been demonstrated as a viable, scalable technology for FSI. A collimated, single-fibre GLI has been constructed and can be used

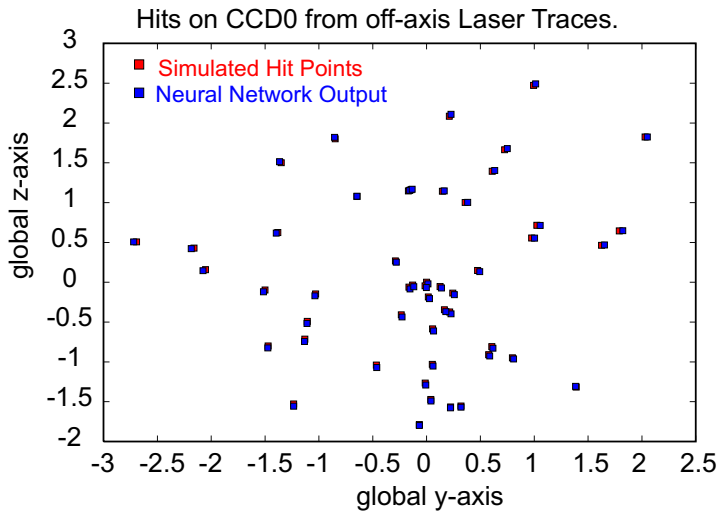

Figure 13: The graph shows the results of the Neural Net simulation to derive an effective parameterisation of the LSM internal geometry. The graph shows the simulated position of one the CCDs (red points). A Neural Net is trained with data from the simulation. It is then asked to determine the CCD's position given only the recorded beam positions.The graph shows the Neural Net has been successful in reconstructing the CCD's position.

for FSI. The analysis algorithms have been developed to take data from the system and be processed to give reliable results.

The next stage for the FSI system is to reduce the measurement errors to 1 μm and to make multi-line measurements. This will require the following to be available:

- A stable evacuated reference interferometer.
- Environmental monitoring of temperatures and pressures of open air GLIs
- Optimisation of the collimation optics
- Improvements to the photodetector electronics to read out lower power FSI signals.
- Continuing development of the analysis algorithms to improve FSI analysis.

The choice of source for the LSM has been shown to be suitable and stable. The beam analysis was shown to be able to measure the beam positions to 1 μm. A half-LSM system was shown to be sensitive to translations and rotations.

The next stage for the LSM development is to operate the LSM on the 4-DOF setup (figure 12). The LSM is mounted on sub-micron and sub-micro radian precision stages. This will allow the LSM sensitivity to be measured and demonstrate whether the LSM can achieve the requirements for the RTRS. Another step for the LSM is the development of the calibration and reconstruction analysis. Two approaches have been pursued for simple

LSM models. The next few months will show which of these methods is most accurate and robust.

In the next year, the FSI and LSM systems are expected to be integrated into a complete LiCAS module. The complete unit will be fixed to a motorised rail in the lab to drive the LiCAS unit to reference markers attached to a fake tunnel wall. This will attempt to measure the reference marker positions under lab conditions. By Autumn 2005, a 3 car prototype RTRS train is scheduled for testing at DESY. This will be first test of a complete train.

References

[1] "TESLA, The Superconducting Electron-Positron Linear Collider with an Integrated X-Ray Laser Laboratory", Technical Design Report, DESY 2001-011.

[2] M. Schlösser, " The Rapid Tunnel Reference Surveyor (RTRS)", 8th International Workshop on Accelerator Alignment, October 2004, CERN, Geneva, Switzerland.

[3] G. Grzelak et al., "Simulation of the LICAS survey system for a next Linear Collider", 8th International Workshop on Accelerator Alignment, October 2004, CERN, Geneva, Switzerland.

[4] A.F. Fox-Murphy et al., "Frequency scanned interferometry (FSI): the basis of the survey system for ATLAS using fast automated remote interferometry", Nuclear Instruments and Methods in Physics Research A 383 (1996) 229-237.

[5] P.A. Coe et al, "Frequency scanning interferometry in ATLAS: remote, multiple, simultaneous and precise distance measurements in a hostile environment", Measurement Science and Technology 15 (2004) 2175-2187 (and references therein)

[6] S. M. Gibson, P. A. Coe, A. Mitra, D. F. Howell, R. B. Nickerson, "Coordinate Measurement in 2-D and 3-D Geometries Using Frequency Scanning Interferometry", Optics and Lasers in Engineering, Accepted for publication.

[7] S. M. Gibson, P. A. Coe, A. Mitra, D. F. Howell, R. B. Nickerson, "Monitoring the heart of ATLAS using Frequency Scanning Interferometry", Proceedings of the Eighth International Workshop on Accelerator Alignment, CERN, Geneva, Oct. 2004.

[8] L. Brunel, "SIMULGEO: Simulation and reconstruction software for optogeometrical systems", CERN CMS Note 1998/079.

[9] R. Brun and F. Rademakers, "ROOT: An object oriented data analysis framework," Nucl. Instrum. Meth. A 389 (1997) 81.

[10] C. C. Davis, "Lasers and Electro-optics: Fundamentals and Engineering", Cambridge University Press, ISBN 0-521-48403-0

[11] USB.org web site, http://www.usb.org

[12] Melles Griot, http://www.mellesgriot.com/